Application of a Bandpass Filter for the Active Vibration Control of High-Speed Rotors

Miroslav Pawlenka, Miroslav Mahdal and Jiří Tůma

Department of Control Systems and Instrumentation at VŠB-TU Ostrava, Czech Republic.

Adam Bureček

Department of Hydromechanics and Hydraulic Equipment at VŠB-TU Ostrava, Czech Republic.

(Received 7 May 2018; accepted 22 November 2018)

This study concerns the active vibration control of journal bearings, which are also known as sliding bearings. The control system contains a non-rotating loose bushing, the position of which is controlled by piezoelectric actuators. For governing the respective orthogonal direction of the journal motion, the control algorithm realizes a proportional controller in parallel with a bandpass filter of the IIR type. The bandpass filter is of the second order and its centre frequency is self-tuned to be the same as the whirl frequency that results from the instability of the bearing journal due to the oil film. The objective of active vibration control is to achieve the highest operational speed of the journal bearing at which the motion of the rotor is stable. The control algorithm for the active vibration control is implemented in Simulink and realized in a dSPACE control system.

NOMENCLATURE

D_n	Denominator determinants
CPB	Constant Percentage Band
f_{rotor}	Rotor rotational frequency
f_{whirl}	Frequency of whirl instability
$G(s)$	Transfer function of the filter
$G(j\omega)$	Frequency transfer function of the filter
IIR	Infinite Impulse Response
I_n	n-order integral for calculating the variance
j	Imaginary unit
K	Gain factor
NASA	National Aeronautics and Space Administration
N_n	Numerator determinants
rpm	Revolutions per minute
s	Complex s-plane
$S_{xx}(\omega)$	Power spectral density
T_0	Time constant
ξ	Damping ratio
ω	Angular frequency
σ_y^2	Variance at the output
σ_x^2	Variance at the input

1. INTRODUCTION

Currently, hydrodynamic sliding bearings are highly advantageous owing to their high radial load and operating loads at high shaft rotation speeds. At high speeds, however, there is an adverse phenomenon. Namely, the excitation of shaft vibrations called an oil whirl. This vibration occurs when the rotational speed exceeds a threshold, which is related to the radial clearance and lubricating oil viscosity. At present, the massive deployment of high-speed hydrodynamic bearings is partially limited by the aforementioned unfavourable vibration phenomenon that can vibrate the entire machine and lead to damage. The vibrations produced when the threshold speed is exceeded due to the oil film properties, as evidenced by theoretical analysis.[1,2] There is a passive approach to suppress the resulting vibrations, such as a structural change of the bearing bushing, e.g., to an elliptical or a lemon form, by creating segments or inserting grooves.

In this study, the focus is on realizing vibration suppression with the use of an active vibration control system, the principle of which is a non-rotating loose bushing, whose position is controlled by piezoelectric actuators also called piezo actuators shortly. For the tests, a test stand was designed to achieve maximum shaft speeds of up to 24 000 rpm. Throughout this range, it was possible to monitor the occurrence of shaft instability by measuring the movements of the bearing journal. The objective of the entire research was to suppress the shaft vibrations and increase the boundary of instability to a higher shaft rotation speed by using a suitable control algorithm and piezoelectric actuators. The entire control algorithm being programmed in the dSPACE control system as a real-time system made it necessary to resolve several other sub-tasks. One of these tasks was to apply an automatically tuneable bandpass second-order filter of the IIR type, which should improve the efficiency of the active vibration control system. The proportional feedback controller provides attenuation of the disturbances over a wide frequency range while the bandpass filter, in parallel with the proportional feedback controller, allows a selective increase of the proportional gain of the controller in the narrow frequency range where the bearing journal tends to vibrate.

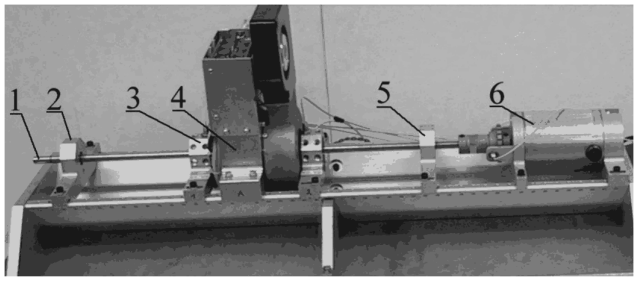

1) rotor, 2) and 5) bearings, 3) displacement transducers, 4) actuator, and 6) driving electrical motor

Figure 1. The test environment in the Jeffcott rotor layout.[3]

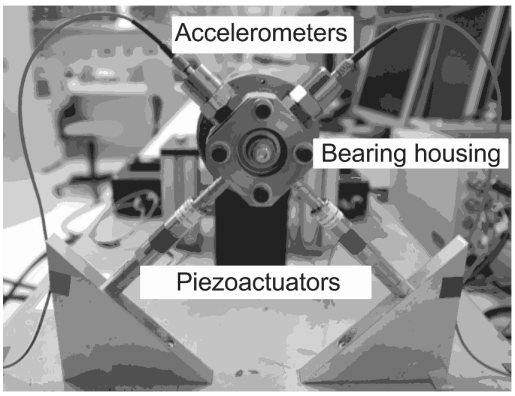

Figure 2. Test stand with piezoelectric actuators.[4]

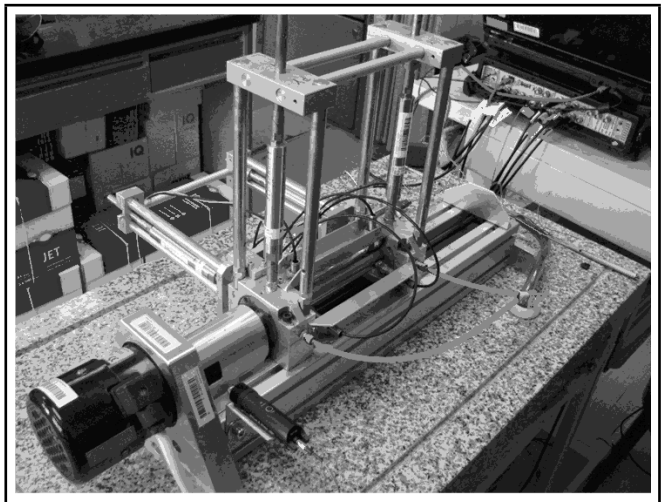

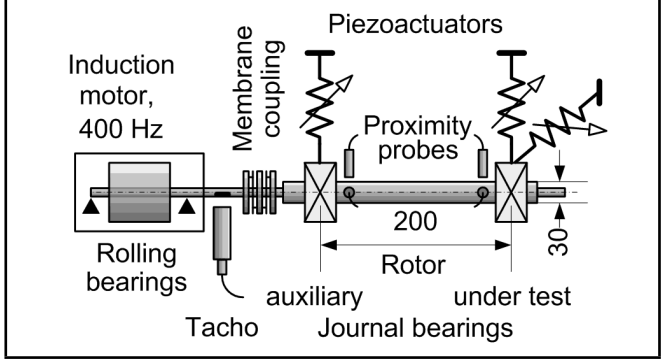

Figure 3. Description of the test stand.

2. PROBLEM DEFINITION

At present, efforts are being made for extending the life of machines and improving their operational efficiency. This requirement is also closely related to active vibration control. Active vibration suppression can lead to longer service life, as well as higher machine rotational speeds. From the industrial perspective, active vibration control is desirable because vibrations are particularly problematic for machine tools, etc. There are requirements for high-precision machining and high-speed cutting.

We now highlight some articles reported worldwide that address this issue. This study described a test device that tested vibration damping using magnetic actuators, see Fig. 1.[3] The magnetic bearing was a part of the Bently Nevada Rotorkit of the RK 4 type. The test device for testing the sliding bearings with active vibration control using piezo actuators is shown in Fig. 2. The literature describes its design.[4] The bearing journal rotated at approximately 5000 rpm. The active vibration control system used a feedback signal, which was the velocity or acceleration of the bearing housing. The bearing was intended to be used in a flywheel for energy storage to achieve long-term service life. The preferred means for rotor control were magnetorheological liquids. However, the delayed response of the liquid viscosity to the magnetic field change didn't allow this method to be used for the closed-loop control of high-speed rotors.[5] The first paper dealing with actively controlled hydrodynamic slide bearings was published in 2002.[6] The vibration damping of hydrodynamic bearings using magnetostrictive actuators, but the usability of the test device was only for low revolution speeds.[7] The article solved the theoretical problem of the stability of the control loop but does not describe a suitable actuator. By the 1990s, NASA had employed piezoelectric pushers (actuators) for active vibration damping.[8] The shaft, in this case, is supported by ball bearings. Development of piezo actuators continues.[9] Literature that focuses on the active vibration control of rotors is reported in publications.[10–13]

The research of the active vibration control of journal bearings that use piezo actuators began at the VSB Technical University of Ostrava and Prague's Techlab Company in 2007.[14] We created an original test facility that uses bearings very similar to their industrial design. The test rig allowed for the testing and verification of control algorithms to efficiently suppress the rotor vibrations due to the rotor motion instability. Piezo actuators were used for the positioning of non-rotating loose bearing bushing.

3. DESCRIPTION OF TEST STAND

The test set-up was composed of a shaft which was supported by two sliding radial hydrodynamic bearings, and it enabled the monitoring of rotor motion and its control as is shown in Fig. 3. The span of bearing pedestals was 200 mm, the bearing diameter was 30 mm, and the length to diameter ratio of the journal bearings was equal to 0.77. For the results presented here, the radial clearance was 55 μm. In operation, the lubricating oil entered under pressure into the gap between the bearing bushing and the journal. The oil inlet was located

in the horizontal plane of the bushing symmetry in the middle of the bearing length. The inner surface of the bushing was smooth without grooves. Special oil for high-speed spindle bearing of the OL-P03 type was used for testing (VG 10 grade). Tests were carried out without preheating the lubricant at a normal temperature.

Measurement of the shaft position relative to the bearing body was carried out in two perpendicular directions rotated by 90 degrees from each other which are also perpendicular to the axis of the shaft. Proximity probes are located near each of two bearings.

The bearing bushing was shifted in the radial direction by the linear piezo actuators of the P-844.60 type. The P-884.60 was a product of the Physik Instrumente Company. The piezo actuator required a low voltage amplifier with the 120 V peak value at the output. The piezo actuator travel range was 90 μm, the pushing force was 3000 N, and the pulling force was 700 N. Piezo actuator holders were designed to eliminate their bending and torsional load. The design of the holder is available in a paper.[15]

The three-phase induction motor drove the rotor. The frequency inverter of the Commander SKA1200075 (Control Techniques) type powered the driving motor. The maximum frequency of the inverter was 400 Hz. Thus, the maximum motor rotational speed was 24 000 rpm. The power of the induction motor of the ATAS FT4C52G type was 500 W. The power of the frequency inverter was 750 W. The laser speed sensor (Tacho) measured up to 250 000 rpm, which suited the specified speed range. The Kalman filter reduced possible small errors of the rotational speed measurement.[16–18]

As it was mentioned, the position of the journal was measured using proximity sensors. The principle of the proximity sensors was based on the capacitive sensors of the capaNCDT CS05 type originated from the MICRO-EPSILON company, see Fig. 4.[19] These sensors had a measuring range of 0.5 mm. The capaNCDT system was based on the principle of the parallel plate capacitor. Changing the distance of the two plates determined the capacitance change of the capacitor. For conductive materials, the tip of the sensor and the shaft surface formed the two electrodes. This theoretical principle was realized almost ideally in practice by designing the sensors as guard ring capacitors. In this case, it dealt with two capacitors. The conductive shaft surface connected these two capacitors in series. The second electrode of both capacitors was connected to a control unit that contained a demodulator. The advantage of this distance measurement solution was that no target grounding was required. If we measured by two sensors simultaneously, both the two control units must be synchronized. The measurement error of the capacitance sensors is less than 1 μm.

The entire layout of the individual elements of the bearing housing body, such as the sensors, the actuators, the bearing bushing and the journal, can be seen in Fig. 5. Active vibration control of the journal bearing enabled the movable bearing bushing. As mentioned above, the bushing did not rotate, and the piezo actuators provided the bushing movement in two radial directions.

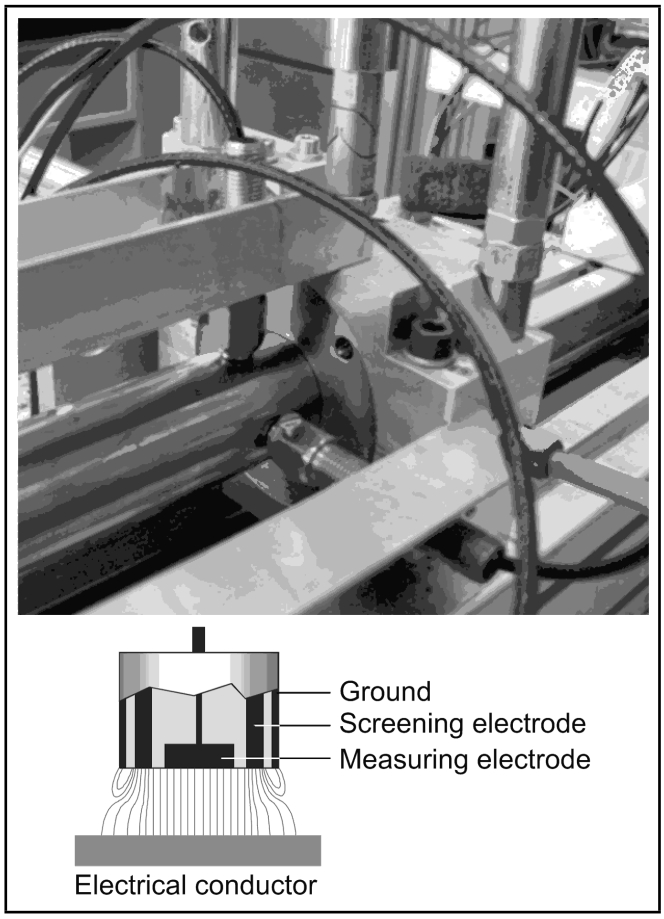

Figure 4. Principle of the capacitive proximity probe.[18]

The desired journal position in the horizontal and vertical directions in a plane perpendicular to the axis of the shaft was compared with the actual position. The calculated control error was transformed by the controller into magnitudes of two manipulated variables, which were the voltages for the piezo actuator amplifiers. All calculations were performed in the dSPACE signal processor. Amplified voltages govern the piezo actuator positions.

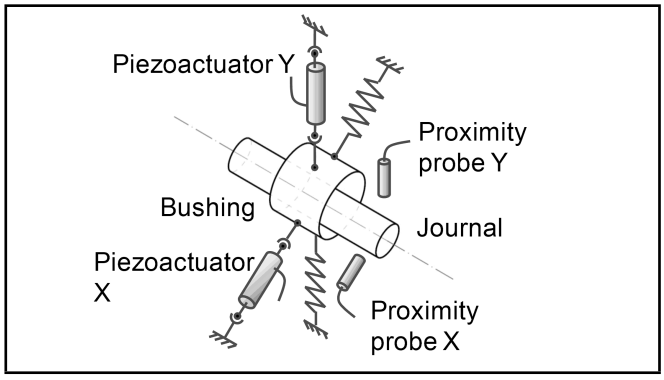

Figure 5. Schematic of the layout of the elements of the journal bearing.

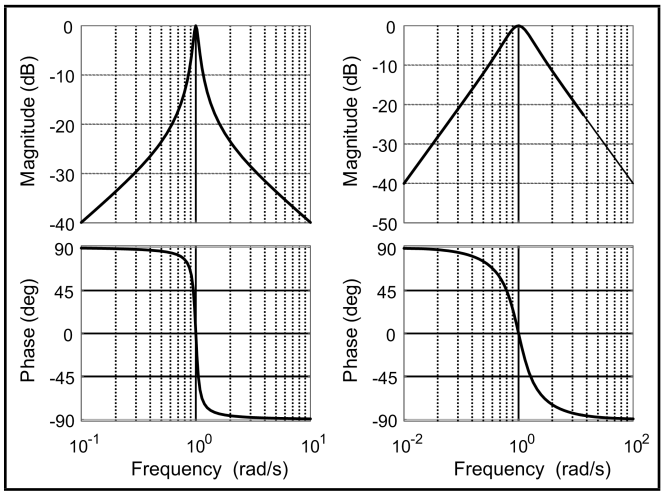

Figure 6. Bode plot of the bandpass filters frequency function $\xi = 0.05$ (left column) and $\xi = 0.5$ (right column).

4. BANDPASS FILTER IN ACTIVE VIBRATION CONTROL

The preceding chapter contains a detailed description of the test rig. Active vibration control has been tested in the past as well.[14,15] Improving the control algorithm has become the focus of doctoral dissertations that discuss the improvement of the signal-to-noise ratio of the feedback signal. The main interest was to prove the theoretical assumptions experimentally.[20]

A bandpass filter belongs to the class of digital filters. Its upper and lower cut-off frequencies limit the bandwidth of a bandpass filter. For the control of active vibration damping, a second-order bandpass filter was used to avoid the unnecessarily long phase delays in the feedback loop. A first order bandwidth filter cannot be designed, and a higher order implies a longer unwanted delay. The Bode plot of the second-order bandpass filter is shown in Fig. 6. When we adapted the filter parameters, the second-order bandpass filter was also tuneable. The purpose of the bandpass filter was to track a disturbance whose frequency changed proportionally to the rotational speed of the rotor.

The second-order bandpass filter has the transfer function

$$G(s) = \frac{Y(s)}{X(s)} = K\frac{T_0 s}{T_0^2 s^2 + 2\xi T_0 s + 1};$$
$$s = j\omega, \qquad \omega = \frac{1}{T_0}, \qquad \omega = 2\pi f_{\text{whirl}}. \tag{1}$$

The frequency function of the bandpass filter to gain $K = 1$ and time constant $T_0 = 1$, and two different damping ratios ξ are plotted in Fig. 6. The gain at the centre frequency of the bandpass filter, at the angular frequency $\omega = 1/T$ was equal to 1. For angular frequency $\omega = 0$ and $\omega \to \infty$, the gain was zero. The width of the permeable frequency band was dependent on the damping ratio ξ.

The next step in verifying the function of this filter was to introduce white noise as an input signal and to calculate the variance of the filter's output signal, i.e., after the signal has passed through the filter in continuous time, see Fig. 7. Now, we will present the derivation and calculation of the integral

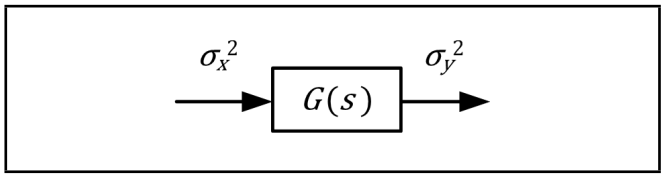

Figure 7. Block diagram of the bandpass filter with white noise at the input of the variance σ_x^2 and the output signal of the variance σ_y^2.

for calculating the variance at the output σ_y^2, which was based on the literature:[21]

$$\sigma_y^2 = \frac{1}{2\pi}\int_{-\infty}^{+\infty} G(j\omega)G(-j\omega)S_{xx}(\omega)d\omega; \tag{2}$$

where $G(j\omega)$ was the cross-spectral density and $S_{xx}(\omega)$ was the power spectral density for white noise and was equal to σ_x^2. Therefore, it was necessary to determine the ratio of the variation in the output to that in the input.

The filter coefficients in the numerator were denoted as $B(s)$ and in the denominator as $A(s)$. Then, we formulated

$$A(s) = T_0^2 s^2 + 2\xi T_0 s + 1 = a_0 s^2 + a_1 s + a_2;$$
$$B(s) = KT_0 s = b_0 s;$$
$$a_0 = T_0^2, \qquad a_1 = 2\xi T_0, \qquad a_2 = 1, \qquad b_0 = KT_0. \tag{3}$$

The substitution of $s = j\omega$ was introduced; the transfer function of the filter had the form

$$G(j\omega) = \frac{jKT_0\omega}{-T_0^2\omega^2 + j2\xi T_0\omega + 1};$$
$$\omega = \frac{1}{T_0}, \qquad G\left(j\frac{1}{T_0}\right) = \frac{K}{2\xi}. \tag{4}$$

The integral for the variance calculation changed after the substitution to

$$\sigma_y^2 = \sigma_x^2\frac{1}{2\pi}\int_{-\infty}^{+\infty} G(s)G(-s)ds. \tag{5}$$

The general formula for calculating the integral in continuous time was

$$I_n = \frac{1}{2\pi j}\int_{-\infty}^{+\infty}\frac{C(s)}{A(s)A(-s)}ds = \frac{1}{2\pi}\int_{-\infty}^{+\infty}\frac{C(j\omega)}{A(j\omega)A(-j\omega)}d\omega. \tag{6}$$

The numerator of the integrated function was calculated as follows

$$C(s) = B(s)B(-s) = \sum_{i=0}^{n-1}\sum_{k=0}^{n-1} b_i b_k s^{i+k}(-1)^k. \tag{7}$$

The filter being second order, $n = 2$, so that

$$C(s) = \sum_{i=0}^{2-1}\sum_{k=0}^{2-1} b_i b_k s^{i+k}(-1)^k = KT_0 s(-KT_0 s);$$
$$C(s) = -K^2T_0^2 s^2 = c_0 s^2, \quad c_0 = -K^2T_0^2, \quad c_1 = 0. \tag{8}$$

The result of the calculation of the integral Eq. (6) was the following formula

$$I_n = \frac{(-1)^{n+1}}{2a_0}\frac{N_n}{D_n}; \tag{9}$$

where the denominator and numerator were determinants

$$D_n = \begin{vmatrix} d_{11} & d_{12} & \cdots & d_{1n} \\ d_{21} & d_{22} & \cdots & d_{2n} \\ \vdots & \vdots & \ddots & \vdots \\ d_{n1} & d_{n2} & \cdots & d_{nn} \end{vmatrix}, \quad D_2 = \begin{vmatrix} d_{11} & d_{12} \\ d_{21} & d_{22} \end{vmatrix};$$

$$N_n = \begin{vmatrix} c_0 & d_{12} & \cdots & d_{1n} \\ c_1 & d_{22} & \cdots & d_{2n} \\ \vdots & \vdots & \ddots & \vdots \\ c_{n-1} & d_{n2} & \cdots & d_{nn} \end{vmatrix}, \quad N_2 = \begin{vmatrix} c_0 & d_{12} \\ c_1 & d_{22} \end{vmatrix}; \tag{10}$$

with individual elements

$$d_{mr} = \begin{cases} a_{2m-r}; & 0 \le 2m-r \le n \\ 0; & 2m-r < 0, \quad 2m-r > n \end{cases};$$

$$d_{11} = \begin{cases} a_{2-1}; & 0 \le 2-1 \le 2 \\ 0; & 2-1 < 0, \quad 2-1 > 2 \end{cases} = a_1;$$

$$d_{22} = \begin{cases} a_{4-2}; & 0 \le 4-2 \le 2 \\ 0; & 4-2 < 0, \quad 4-2 > 2 \end{cases} = a_2;$$

$$d_{21} = \begin{cases} a_{4-1}; & 0 \le 4-1 \le 2 \\ 0; & 4-1 < 0, \quad 4-1 > 2 \end{cases} = 0;$$

$$d_{12} = \begin{cases} a_{2-2}; & 0 \le 2-2 \le 2 \\ 0; & 2-2 < 0, \quad 2-2 > 2 \end{cases} = a_0. \tag{11}$$

After being assigned to the determinants

$$D_2 = \begin{vmatrix} 2\xi T_0 & T_0^2 \\ 0 & 1 \end{vmatrix} = 2\xi T_0;$$

$$N_2 = \begin{vmatrix} -K^2 T_0^2 & T_0^2 \\ 0 & 1 \end{vmatrix} = -K^2 T_0^2. \tag{12}$$

Now, these expressions were used in a relationship for calculating the integral, which may be considered as a bandwidth ratio given by the quotient between the variances of the filter's output and input signals, according to:

$$I_2 = \frac{\sigma_y^2}{\sigma_x^2} = \frac{K^2}{4\xi T_0}. \tag{13}$$

The maximum bandpass filter gain at resonance was as follows:

$$G\left(j\frac{1}{T_0}\right) = \frac{jK}{-1+j2\xi+1} = \frac{K}{2\xi}. \tag{14}$$

If a bandpass filter was not used, it would be necessary to set the gain for the proportional controller to compensate for the bandpass filter. The variance of the input noise at the output of the proportional feedback increased $(K/2\xi)^2$ times. With the bandpass filter, it increased only $K^2/4\xi T_0$ times. The ratio of both the ratios is equal to ξ/T_0. The noise power at the bandpass filter output relating to the noise power at the input was limited by ξ/T_0 times. The bandpass filter improves the signal to noise ratio.

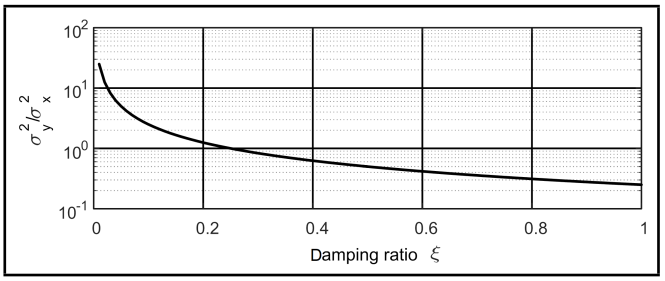

Figure 8. Variances ratio between output and input signal as a function of the damping ratio ξ.

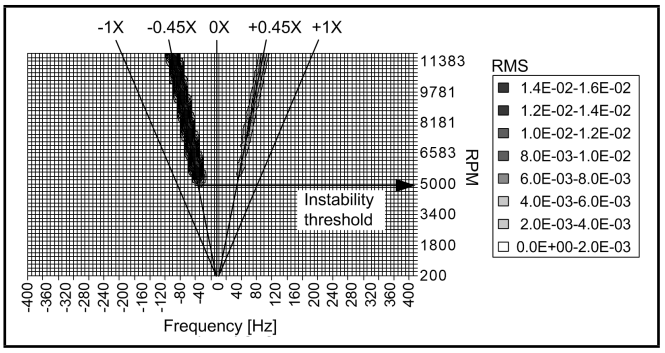

Figure 9. The full cascade spectrum of the journal motion during run-up.

The filter effect was such that the other noise frequency of the filter tuning frequency did not reach the manipulated variable. Therefore, the operation is expected to be quieter.

The bandwidth depended on the damping ratio ξ. Therefore, we plotted the dependence of the variance ratio on damping ratio ξ.

To plot the ratio of the variances in Fig. 8, the values of K and T_0 were set to 1. These values affected the amplitude of the filtered signal.

5. APPLICATION OF THE FILTER

Rotor instability of the whirl type referred to a phenomenon in which the journal axis circulates within the bearing bushing at a reduced speed relative to the rotor rotational speed f_{rotor}.[22] The frequency of the mentioned circulation was named f_{whirl}. This frequency depends on the journal's frequency according to this approximate formula

$$f_{\text{whirl}} = (0.42 \text{ to } 0.48) \times f_{\text{rotor}}. \tag{15}$$

The full cascade spectrum of the journal axis motion for a run-up from 0 to 12 000 rpm is shown in Fig. 9. The spectra demonstrated the presence of a frequency of whirling in the measured signals during increasing rpm after crossing the threshold of instability. The full spectrum was calculated using the FFT for the coordinates of the journal axis in a complex plane that was perpendicular to the journal axis. For example, the FFT time signal decomposed the signal to harmonic components; the full spectrum represented the decomposition of the journal

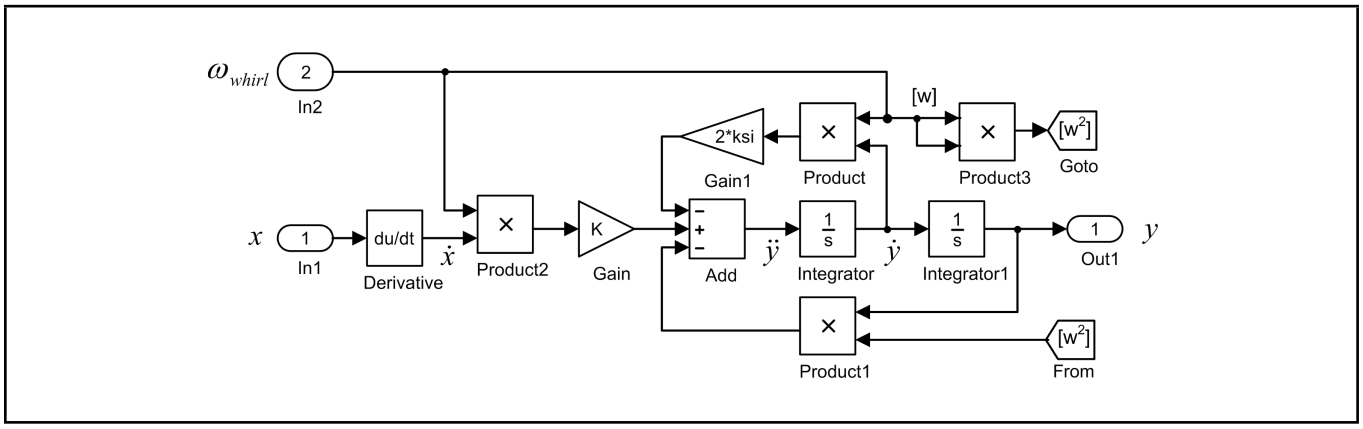

Figure 10. Simulink model of the bandpass filter.

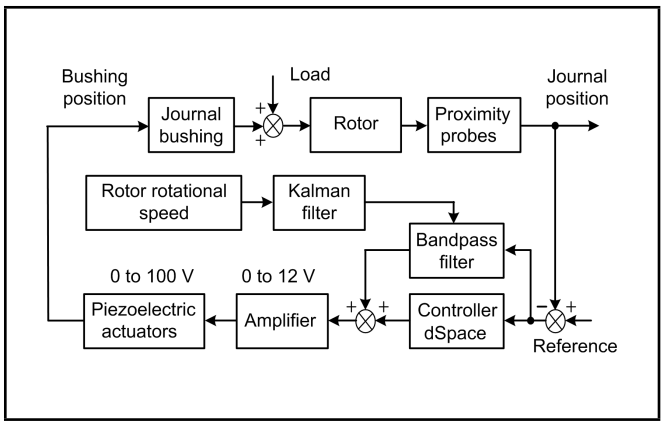

Figure 11. The system of active vibration control system with a bandpass filter.

motion inside the bearing bushing bore on elementary orbits with different rotational frequencies, see a book.[16] The positive frequencies corresponded with the phasor rotation in the positive direction, and the negative frequencies corresponded with the phasor rotating in the opposite direction. An example of the full spectrum of the journal motion without any control demonstrated the elementary orbits of the journal axis, which rotated at $\pm 0.45X$ fraction of the rotor rotational speed. The onset of the instability of the whirl type was excited by a disturbance at that frequency. It was a reason for closing the feedback only for the narrow frequency band around the f_{whirl} frequency, which also increased the signal-to-noise ratio for the feedback signal.

The f_{whirl} frequency was the centre frequency to which the bandpass filter was tuned. The rotors supported on the journal bearings were not operated at a constant rotational speed, so automatically adapting the centre frequency of the bandpass filter was required after rotor speed changes. The bandpass filter of the active vibration control system was realized in the time domain by Simulink, which was implemented in dSPACE. The Laplace transfer function, given by Eq. (1), had to be converted to the second-order differential equation with coefficients which depend on the centre frequency as well. After conversion, the mathematical model of the filter was given

Table 1. Motion stability margins.

Feedback	Out of control	Bandpass filter	Proportional control	Proportional control and bandpass filter
Stability margin	less than 3000 rpm	6500 rpm	7400 rpm	9300 rpm

by the following differential equation:

$$\frac{d^2y}{dt^2} = (0.45 \times 2\pi f_{\text{rotor}})^2 \left[\frac{K}{0.45 \times 2\pi f_{\text{rotor}}} \frac{dx}{dt} - \frac{2\xi}{0.45 \times 2\pi f_{\text{rotor}}} \frac{dy}{dt} - y \right]. \quad (16)$$

As can be seen in Fig. 10, the bandpass filter is directly programmed in the Simulink environment. The input for the filter reset is omitted to make block diagram simpler. The gain K and damping ratio ξ (ksi) were considered as constants. The expression of $0.45 \times 2\pi f_{\text{rotor}}$ was replaced by the identical ω_{whirl} angular frequency. By decreasing the value of the damping ratio ξ, the width of the bandpass of the filter also decreased. The implementation of the bandpass filter in the control algorithm is depicted in Fig. 10. The block diagram of active vibration control is shown in Fig. 11. Parallel connection of the bandpass filter and proportional controller allowed for experimentation with the weighting factors of these feedbacks.

6. EXPERIMENTS

The instability of the rotor motion resulted from the property of the oil film. The operating range of the journal bearing speed was extended by the use of active vibration control, i.e., by introducing feedback between the position of the journal and the bushing. There were three possible combinations for the arrangement of the controller feedback. The experiment enabled the determining of the type of feedback that maximizes the operating speed range. The time ramp at a constant rate of the rpm increase was selected as a set point of the control loop. To compare the effectiveness of active vibration control with operation without this system, it was necessary to specify the maximum possible rotor speed without vibration of the whirl type. Almost every time the instability of the journal motion

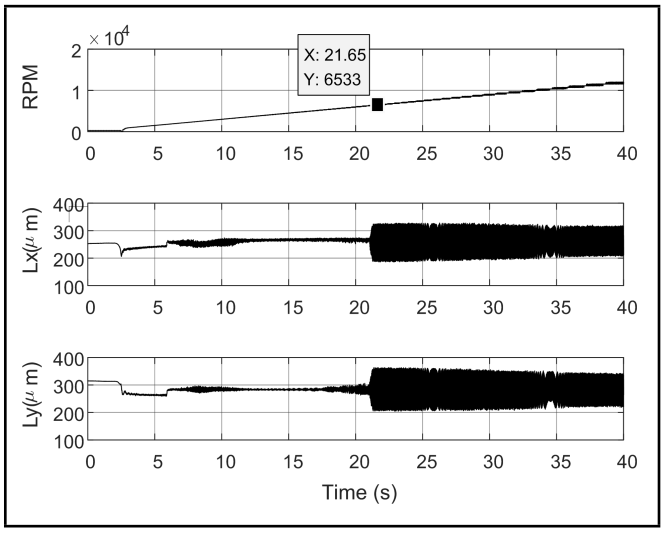

Figure 12. Active vibration control with the bandpass filter only.

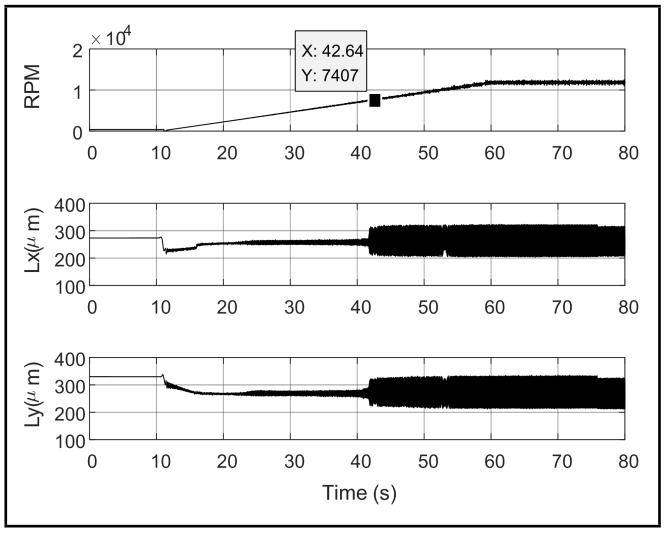

Figure 13. Active vibration control with the proportional controller only.

occurred before reaching a speed of 3000 rpm. During the unstable movement, the bearing journal moved in an almost circular path with a diameter that was given by clearance in the bearing. Many tests confirmed that the movement of the bearings in the bushing is unstable when the rotational speed exceeds the limit of 2500 rpm. Radial clearance and oil temperature were the same.

As mentioned above, different combinations of the connections of the bandpass filter and proportional controller were tested. Here are the measurements for the controller parameters that led to the best results. Figure 11 shows the control with bandpass filters without the parallel proportional controller (the gain of the proportional controller is set to 0). Instability of the journal motion occurs when 6553 rpm is exceeded. The cursor indicates the onset of instability in Figs. 12, 13 and 14. Variable X of the cursor data was the time in seconds and Y was the value in rpm for diagrams showing the stability margin. The scale for the vertical position of the bearing journal was in reverse order to show the visible upward stroke of the rotor axis after the run-up.

In the proportional control, the instability occurred after crossing approximately 7407 rpm. In Fig. 13, the control only with the proportional controller is presented. In Fig. 14, the control with the combination of the proportional controller and the bandpass filter is presented. By combining the proportional controller and the bandpass filter, the best results are achieved. Table 1 lists the results of the experiments. It becomes clear that active vibration control is adapted to improve the functional properties of bearings by applying electronics to replace passive measures against whirl vibration that cannot be easily and inexpensively manufactured in comparison to the cylindrical bushing. The prototype of an actively controlled bearing is the first fully functional device in the world.

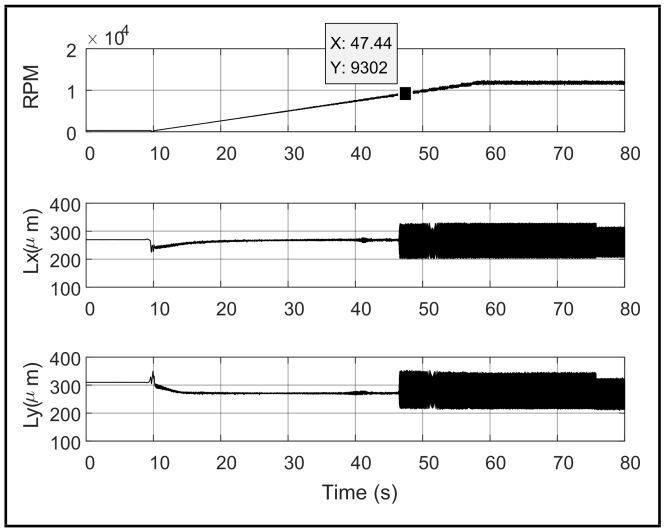

Figure 14. Active vibration control with the combination of the bandpass filter and the proportional controller.

7. CONCLUSIONS

This article describes the implementation of the proportional controller and the second-order bandpass filter to compensate disturbances in a limited frequency band. The bandpass filter increases the feedback gain in the narrow frequency band and, in this way, increases the threshold rotation speed at which the 'whirl' type instability occurs. The experiments proved that the filter has a positive effect on active vibration control. The highest rotational speed at stable operation (approximately 9300 rpm) was obtained by combining the proportional controller and the bandpass filter. The stable operational range is three or four times greater than for the sliding bearing without any active vibration control. With the use of the proportional feedback and without the filter, we could achieve a speed of approximately 7400 rpm. The Kalman filter smoothes the instantaneous rotational speed signal that inputs to the bandpass filter because the measurement of rpm is a lightly corrupted by a random error. The speed is evaluated from the tacho-signal, which is a string of pulses. The linear interpolation of the trigger level with the rising edge of the pulses enhances the calculation of the length of the time interval between the pulses of the tacho-signal.

ACKNOWLEDGEMENTS

This work was supported by the European Regional Development Fund in the Research Centre of Advanced Mechatronic Systems project, project number CZ.02.1.01/0.0/0.0/16_019/0000867 within the Operational Programme Research, Development and Education.

REFERENCES

[1] Muszynska, A. Whirl and whip—Rotor/bearing stability problems, *Journal of Sound and Vibration*, **110** (3), 443–462, (1986). https://dx.doi.org/10.1016/S0022-460X(86)80146-8

[2] Muszynska, A. *Rotordynamics*, Taylor & Francis Group, New York, (2005).

[3] Tammi, K. Active vibration control of rotor in a desktop test environment, *Espoo 2003*, VTT Publications 498, (2003).

[4] Zisser, M., Schweighofer, B., Wegleiter, H., Haidl, P., and Bader, M. Test rig for active vibration control with piezo-actuators, *Proceedings of the 22nd International Congress on Sound and Vibration—Book of Abstracts*, Florence, 2015.

[5] Zapoměl, J., Ferfecki, P., and Kozánek, J. Modelling of magnetorheological squeeze film dampers for vibration suppression of rigid rotors, *International Journal of Mechanical Sciences*, **127**, 191–197, (2017). https://dx.doi.org/10.1016/j.ijmecsci.2016.11.009

[6] Rho, B.-H. and Kim, K.-W. The effect of active control on stability characteristics of hydrodynamic journal bearings with an axial groove, *Proceedings of the Institution of Mechanical Engineers, Part C: Journal of Mechanical Engineering Science*, **216** (9), 939–946, (2002). https://dx.doi.org/10.1177/095440620221600907

[7] Lau, H. Y., Liu, K. P., Wang, W., and Wong, P. L. Feasibility of using GMM based actuators in active control of journal bearing system, *Proceedings of the World Congress on Engineering 2009*, **II**, London, U.K., (2009).

[8] Palazzolo, A. B., Lin, R. R., Alexander, R. M., Kascak, A. F., and Montague, J. J. Piezoelectric Pushers for Active Vibration Control of Rotating Machinery, *Journal of Vibration, Acoustics, Stress, and Reliability in Design*, **111** (3), 298–305, (1989). https://dx.doi.org/10.1115/1.3269856

[9] Płaczek, M. Modelling and investigation of a piezo composite actuator application, *International Journal of Materials and Product Technology*, **50** (3–4), 244–258, (2015). https://dx.doi.org/10.1504/IJMPT.2015.068532

[10] Pinte, G., Devos, S., Stallaert, B., Symens, W., Swevers, J., and Sas., P. A piezo-based bearing for the active structural acoustic control of rotating machinery, *Journal of Sound and Vibration*, **329**, 1235–1253, (2010). https://dx.doi.org/10.1016/j.jsv.2009.10.036

[11] Mizumoto, H., Arii, S., Yabuta, Y., and Tazoe, Y. Vibration control of a high-speed air-bearing spindle using an active aerodynamic bearing, *International Conference in Control, Automation and Systems 2010*, Gyeonggi-do, Korea, (2010). https://dx.doi.org/10.1109/ICCAS.2010.5669831

[12] Carmignani, C., Forte, P., and Rustighi, E. Active control of rotor vibrations by means of piezoelectric actuators, *Proceedings of DETC'01, ASME 2001 Design Engineering Technical Conference and Information in Engineering Conference*, 757–764, (2001).

[13] Lebo, F. and Rinderknecht, S. Modellbasierte Regelung eines skalierten elastichen Flugtribwerkrotors mit Piezostapelaktoren, *Proceedings of SIRM 2011—9th International Conference on Vibrations in Rotating Machines*, Paper-ID: 27, Darmstadt, Germany, (2011).

[14] Tůma, J., Šimek, J., Škuta, J., and Los, J. Active vibrations control of journal bearings with the use of piezo actuators, *Mechanical Systems and Signal Processing*, **36** (2), 618–629, (2013). https://dx.doi.org/10.1016/j.ymssp.2012.11.010

[15] Tůma, J., Šimek, J., Mahdal, M., Škuta, J., and Wagnerová, R. Actively controlled journal bearings, *Proceedings of SIRM 2017—12th International Conference on Vibrations in Rotating Machines*, 443–462, Graz, Österreich, (2017).

[16] Tůma, J. *Vehicle Gearbox Noise and Vibration: Measurement, Signal Analysis, Signal Processing and Noise Reduction Measures*, Wiley, Hoboken, N.J., (2014).

[17] Pawlenka, M. and Mahdal, M. CompactRIO control system for active vibration control, *Proceedings of the 19th International Carpathian Control Conference ICCC 2018*, 134-137, Hungary, (2018). https://dx.doi.org/10.1109/CarpathianCC.2018.8399616

[18] Tůma, J. Rotational speed estimation using the discrete Kalman filtering applied to a tacho signal, *Proceedings of the 19th International Carpathian Control Conference ICCC 2018*, 39–44, Hungary, (2018). https://dx.doi.org/10.1109/CarpathianCC.2018.8399599

[19] CapaNCDT sensors. Product datasheets. Retrieved from https://www.micro-epsilon.com/download/products/cat--capaNCDT--en.pdf, (Accessed February 1, 2018).

[20] Pawlenka, M. The use of microcomputers for the real-time control of systems with fast response (Využití mikropočítačů pro řízení systémů s rychlou odezvou v reálném čase), Doctoral Dissertation, VSB—Technical University of Ostrava, Ostrava, (2018).

[21] Tůma, J. *Stochastic Control Theory* (in Czech), VSB—Technical University of Ostrava, Ostrava, (1998).

[22] Pawlenka, M. and Mahdal, M. Automatically tunable bandpass filter, *Proceedings of the 18th International Carpathian Control Conference ICCC 2017*, 7970391, 167–170, Romania, (2017). https://dx.doi.org/10.1109/CarpathianCC.2017.7970391